Journal of Pharmaceutical Sciences 110 (2021) 1292-1301

Contents lists available at ScienceDirect

Journal of Pharmaceutical Sciences

journal homepage: www.jpharmsci.org

Pharmaceutics, Drug Delivery and Pharmaceutical Technology

Probing Microenvironmental Acidity in Lyophilized Protein and Vaccine Formulations Using Solid-state NMR Spectroscopy

Mingyue Li [a, e], Sampada Koranne [a, e], Rui Fang [a, e], Xingyu Lu [a, f], Donna M. Williams [b], Eric J. Munson [c], Akhilesh Bhambhani [b, **], Yongchao Su [a, c, d, *]

[a] Pharmaceutical Sciences, Merck & Co., Inc, Kenilworth, NJ 07033, USA
[b] Vaccine Drug Product Development, Merck & Co., Inc, West Point, PA 19486, USA
[c] Department of Industrial and Physical Pharmacy, College of Pharmacy, Purdue University, IN 47907, USA
[d] Division of Molecular Pharmaceutics and Drug Delivery, College of Pharmacy, The University of Texas at Austin, Austin, TX 78712, USA

ARTICLE INFO

Article history:
Received 20 September 2020
Revised 25 October 2020
Accepted 16 November 2020
Available online 26 November 2020

Keywords:
Protein formulation
Vaccine
Lyophilization
Stability
Microenvironmental acidity
Histidine
Solid-state NMR

ABSTRACT

Biophysical and biochemical instability of therapeutic proteins in the solution state may necessitate the development of products in the solid form, due to their enhanced stability. Lyophilization is a widely used method to ensure dry state stabilization of biological products. A commonly encountered issue is the pH shifts that can occur due to undesired crystallization of a buffer component, resulting in loss of protein activities. However, it is technically challenging to noninvasively investigate the physicochemical environment in the lyophile matrix. In this work, we demonstrate an approach based on solid-state NMR to investigate the microenvironmental acidity in lyophilized protein formulations, using histidine, a commonly used buffer agent, as a molecular probe. The solid-state acidity in the lyophilized matrix can be assessed by monitoring the chemical shift changes of histidine. The protonation and tautomeric states of histidine lyophilized at a range of pH values from 4.5 to 11.0 were identified from full ^{13}C and ^{15}N resonance assignments in one-dimensional and two-dimensional NMR experiments. The results demonstrated a pH-dependence of histidine chemical shift in the amorphous state. Moreover, we successfully applied this protocol to investigate the microenvironmental pH in lyophilized formulations of the HPV vaccine and lactate dehydrogenase protein.

Introduction

Lyophilization has become a major platform to prepare solid formulations of proteins and vaccines. Drying processes involve various thermal, dehydration, and mechanical stresses, which can impact stability of protein formulations differently.[1] Therefore, major tasks in the formulation development are to optimize the drying process and rationalize the selection of excipients. The stability and performance of the lyophilized product can be dictated by the physical form of the drug substances and excipients. Protein therapeutics are often formulated in buffered solution and stored in frozen or freeze-dried state, which may contain excipients such as a buffer, stabilizer, tonicity modifier, and a bulking agent.[2] A buffer solution is used to maintain the pH of the formulation in the working range throughout its shelf-life. Common buffers for protein formulations include phosphate, acetate, histidine, citrate, and tris.[3] The controlled acidity plays an important role in determining the stability of proteins, antibiotics, and vaccines in frozen and freeze-dried formulations. A change of pH in the formulation during production and storage may cause stability issues when the active ingredient or excipient undergo degradation at pH values different from the original aqueous pH.[4–9] Selective crystallization of buffer components during freezing and freez-drying can result in unexpected pH changes, which depends on factors such as buffer concentration, cooling rate, temperature, and initial pH.[10] Dramatic pH shifts induced by buffer crystallization during freeze-thaw cycling in phosphate buffered solutions have been reported to cause the aggregation of bovine serum albumin and beta-galactosidase.[11] A detrimental effect of pH shift was also observed on lactate dehydrogenase (LDH) and a model enzyme upon freezing.[11,12] The pH shift due to buffer salt crystallization can be

* Corresponding author. Pharmaceutical Sciences, Merck & Co., Inc, Kenilworth, NJ 07033, USA.
** Corresponding author.
E-mail addresses: akhilesh_bhambhani@merck.com (A. Bhambhani), yongchao.su@merck.com (Y. Su).
[e] M.L., S.K., and R. F. have equal contributions.
[f] Current address: Instrumentation and Service Center for Physical Sciences, Westlake University, Hangzhou, Zhejiang, 310024, China.

https://doi.org/10.1016/j.xphs.2020.11.017
0022-3549/

adversely affected by including non-crystallizing solutes such as sugar, polymers and proteins.[13] The addition of trehalose, by inhibiting buffer crystallization, has been reported to prevent pH shift upon the freezing.[14] Therefore, the knowledge of pH stability in formulations during lyophilization and storage is critical to the drug development of proteins and vaccines.[15]

Since the 1990s, the importance of microenvironmental pH (pH_M) of pharmaceutical solids to drug development has been discussed due to its significant impact on drug stability and dissolution.[16–18] pH_M is sometimes described as the pH of the saturated solution on the immediate surface of the drug particle.[19] Modulating the pH_M of matrix systems by incorporation of pH modifiers can help improve controlled release of weakly ionizable compounds.[19–21] Tremendous efforts have been carried out to develop reliable techniques to determine pH_M in the solid state.[22] The pH measurement of a slurry may closely represent solid surface pH.[23] An indicator dye-sorption method can probe solid surface acidity and can enable rank ordering of acidity in systems based on the ionization state of the indicator dye molecule. However, a comparison of the dye-sorption and slurry pH method showed partial disagreement depending on the compound and the indicator.[24] It has been demonstrated that pH measurement based on calibration plots of aqueous dye solution is not applicable to the solid state in many cases.[24] Electron paramagnetic resonance (EPR) imaging is used to evaluate pH_M inside tablets by incorporating pH-sensitive spin labels.[21] Confocal laser scanning microscopy has been used to map the spatial distribution of pH_M using pH-sensitive fluorophore.[25] One direct method to potentiometrically determine the pH on the surface is established by using a surface pH electrode.[19,26] Most existing pH measurements of solids are based on introducing exogenous chemicals which may disturb the microenvironmental acidity and affect stability of drug products. An alternative, non-invasive method to measure in situ acidity of lyophilized products will benefit the development of drug products when electrochemical or spectroscopic measurements are not feasible or ambiguous.

For example, Gardasil and Gardasil®9 are vaccines against the most prevalent types of human papillomaviruses and have been shown to be effective in preventing HPV-related cancers. The vaccines are composed of virus-like particles (VLPs) expressed and purified from yeast and absorbed to aluminum adjuvant with Gardasil comprising Types 6, 11, 16 and 18 and Gardasil®9 comprising Types 6, 11, 16, 18, 31, 33, 45, 52 and 58.[27,28] These current marketed vaccines are liquid formulations and are stable for up to 2 years at 2–8 °C. The utilization of lyophilization can enhance the thermostability of type 6, 11, 16, and 18.[29] With the wide development of lyophilized formulations, it becomes urgent to develop method to monitor potential pH changes upon lyophilization. The lyophilization process includes three steps, namely freezing often with annealing, primary drying via ice sublimation, and secondary drying via water desorption. pH values of a frozen solution can be measured by low-temperature pH electrodes operating at sub-zero temperatures to −30 °C.[10,11,14,30] The pH of frozen solutions can also be measured by adding a universal pH indicator solution.[31,32] An earlier study suggested pKa values of model organic compounds containing common functional groups of amino acids are similar in both aqueous and lyophilized forms by Fourier-transform infrared spectroscopy.[33] The concept of "pH memory" of biomolecules was therefore proposed suggesting the behavior of the freeze-dried form corresponds to the pH of the aqueous solution where they were prepared from.[33] However, a robust and non-invasive method is needed to probe the stability as represented by microenvironmental acidity in the solidified biological products as a result of water removal.

Histidine is one of the most commonly used buffers in protein formulations with important functions of regulating shifts of pH as well as stabilizing proteins.[34] The acid-base properties of histidine makes it a good candidate as a pH indicator. Histidine has four potential protonation sites, namely the carboxylate end, two nitrogen atoms of the imidazole ring, and the amine terminal. The successive deprotonation of the carboxylic acid group, imidazolium cation and amine nitrogen has pKa values of 1.9, 6.1 and 9.1, respectively as shown in Fig. 1A. The protonation state of histidine is very sensitive to small changes in the environmental pH.[35–37] At low acidic pH, histidine carries two positive charges. As pH increases, the carboxylic acid group first becomes deprotonated followed by the neutralization of the imidazolium group. As pH increases, the backbone amine group can lose a proton to give an anionic histidine. The neutral imidazole of histidine exists in a pH-dependent equilibrium of two neutral tautomers, the $N_{\varepsilon 2}$-

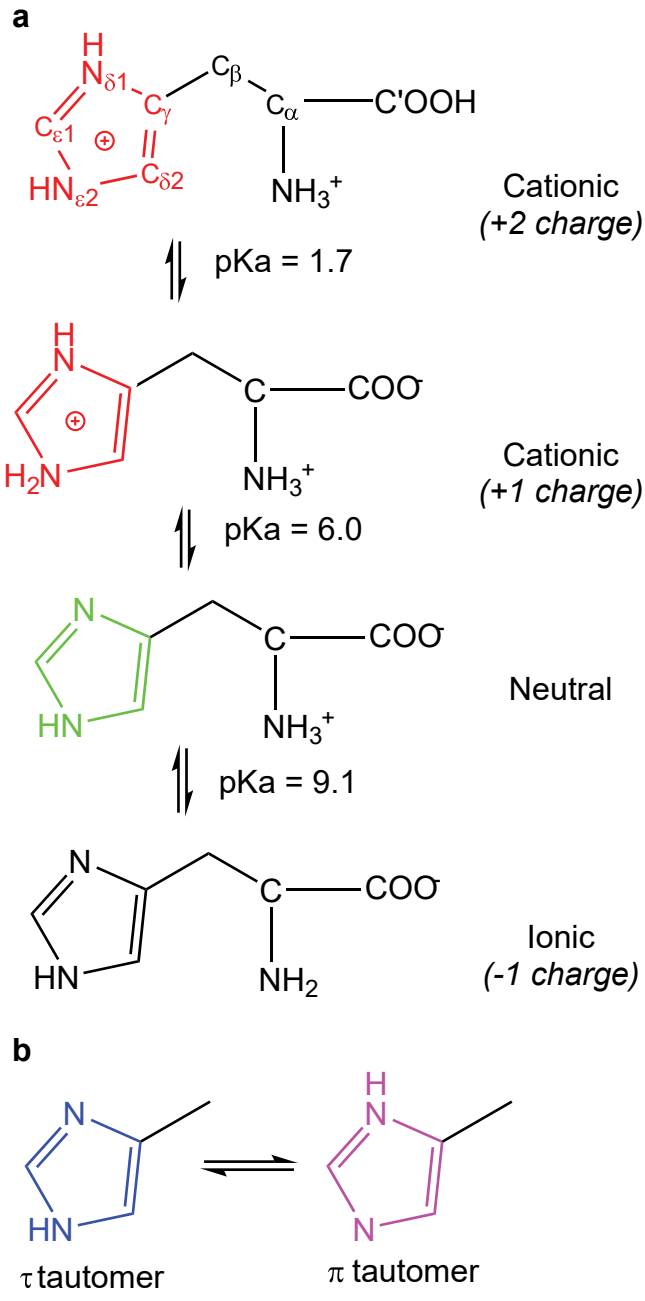

Fig. 1. (a) Protonation states of histidine; and (b) tautomerization of the imidazole ring.

protonated τ tautomer and the $N_{\delta1}$-protonated π tautomer in Fig. 1B. The two forms undergo interconversion through tautomerization and ring flip. The $N_{\varepsilon2}H$ form is favored by ~4 to 7-fold over the $N_{\delta1}H$ form in the neutral imidazole of the amino acid.[36] Since the protonation state and tautomeric conformation of histidine are sensitive to environmental pH, all the ^{13}C and ^{15}N chemical shifts show substantial pH-dependence.[37] In particular, the ring $N_{\delta1}$ and $N_{\varepsilon2}$ have substantially different chemical shifts in their protonated or deprotonated states. $C_{\varepsilon1}$, $C_{\delta2}$ and C_{γ} chemical shifts are also sensitive to the ionization and tautomerization state of histidine, due to the local electronic environmental changes. The pH-dependent distribution of tautomers of a neutral histidine can be deduced upon assignment of its ring ^{15}N and ^{13}C signals. Chemical shifts of crystalline histidine upon ionization and tautomerization have been reported by solution[36,37] and solid state NMR.[35,38] Hong and co-workers showed chemical shift changes of ^{13}C and ^{15}N with an increasing pH provide a robust indication of the tautomeric states at a given pH.[29] Fu and co-workers used ^{15}N selectively ^{13}C ssNMR to identify a mixture of neutral and charged states in a sample of ^{13}C, ^{15}N labeled histidine powder lyophilized from a solution at pH 6.3.[38] In a previous solid state NMR study of lyophilized histidine, Henry et al. showed that chemical shifts of histidine contains the pH information of the parent solutions.[39] However, the dependence of chemical shifts on pH changes of amorphous histidine in complex pharmaceutical formulations has not yet been reported.

Solid-state NMR spectroscopy (ssNMR) has been increasingly utilized as a high-resolution technique to characterize the stability, mobility, and miscibility of lyophilized protein formulations for its capabilities on structural characterization of materials that are lack of long-range order.[40–42] In this work, for the first time, we demonstrate the utilization of histidine in lyophilized formulations as an indicator to probe pH change in lyophilized protein solids by ssNMR. 1D ^{13}C, ^{15}N and 2D ^{13}C–^{13}C homonuclear and ^{15}N–^{13}C heteronuclear correlation spectra are utilized to assign the chemical shifts of amorphous histidine in formulations. Chemical shifts of the imidazole ring are shown to be sensitive to the pH of pre-lyophilized solution. The trend of ^{13}C and ^{15}N chemical shifts with pH from 4.5 to 11 is established. We also investigate the impact of sodium phosphate on chemical shifts of histidine at different pH values. We demonstrate the robustness of this method in model HPV vaccine and LDH formulations.

Materials and Methods

Materials

Chemicals including L-histidine, $^{13}C_6$ and $^{15}N_3$ isotopically labeled L-histidine, polysorbate 80, sodium chloride, trehalose dihydrate and LDH (from rabbit muscle (EC 1.1.1.27), a suspension in 3.2 M ammonium sulfate) were purchased from Sigma-Aldrich. HPV33 VLPs were manufactured by Merck & Co, Inc (West Point, PA). Phosphate buffer were prepared freshly by dissolving the monosodium and disodium phosphate salts in the appropriate ratios to obtain the desired pH and buffer concentration.

Preparation of Lyophilized Histidine With and Without LDH

Pre-lyophilization solutions without LDH were prepared by adding trehalose (5% w/v) and $^{13}C_6$, $^{15}N_3$ L-histidine (20 mM) to sodium phosphate buffer solutions (100 mM or 20 mM; pH 4.5, 6.0, 7.0, 8.0, 11.0). LDH was dialyzed against 100 mM sodium phosphate buffer (pH 7.5) with a 10 K MWCO membrane for 3 h twice and the third buffer exchange for overnight at 4 °C. The concentration of LDH was determined using SoloVPE (Bridgewater, NJ). The extinction coefficient of LDH from rabbit muscle is1.44 mL/mg-cm at 280 nm. The LDH solution was subsequently formulated to a final composition with 10 μg/mL of LDH in 100 mM phosphate buffer (pH 7.5), 20 mM labeled histidine and 50 mg/mL trehalose. Two milliliters of the sample solution were filled into each 10-mL vial (for a fill depth of 0.53 cm) and were partially stoppered with rubber stoppers.

LyoStar 3 (SP scientific, Gardiner, NY) was used for the freeze-drying studies. All sample vials were placed on the center position of the shelf surrounded by empty vials. During freezing, the samples were equilibrated in the freeze-dryer at 5 °C for 30 min, then the shelf was cooled to −40 °C at 1 °C/min and held for 2 h. For primary drying, the chamber pressure was set at 100 mTorr and the shelf was heated at 0.2 °C/min to −25 °C and held constant. When the Pirani gauge signal converges with the capacitance manometer, the shelf temperature was raised to 40 °C at 0.1 °C/min and held for 5 h to complete secondary drying. The samples were backfilled with dry filtered nitrogen to 600 Torr, stoppered and sealed until further analysis.

Preparation of Lyophilized HPV33 VLPs

A placebo formulation at 2× the desired concentration was prepared (20 mM L-histidine, 45.7 mM $^{13}C_6$, $^{15}N_3$ L-histidine, 650 mM sodium chloride, 0.02% polysorbate 80, 10% trehalose). This 2× formulation was split into three separate containers and pH was adjusted to 4.5, 6, and 8, with either 1 M NaOH or 1 M HCl. The formulation was then diluted 1:1 by addition of the appropriate volume of HPV33 VLPs and water (to QS) to make the final formulations (0.54 mg/mL HPV33, 10 mM L-histidine, 22.9 mM 13-C6, 15-N3 L-histidine, 325 mM sodium chloride, 0.01% polysorbate 80, 5% trehalose. The final pH was confirmed for the three formulations as 4.5, 6.0 and 8.0. Formulations were filled into ISO2R vials at a volume of 1 mL each, half stoppered with igloo stoppers, frozen at −115 °C for 15 min, then placed on a −50 °C LyoStar 3 shelf. The shelf was held at −50 °C for 2 h. For primary drying, the chamber pressure was set at 50 mTorr and the shelf was heated at 0.1 °C/min to −25 °C and held for 30 h. The shelf temperature was then raised to 25 °C at 0.1 °C/min and held for 5 h. The samples were backfilled with dry filtered nitrogen to 540 Torr, stoppered and sealed until further analysis. The weight % of the lyophilized HPV33 cakes were 0.721% HPV33 VLPs, 2.07% L-histidine, 5.00% 13-C6, 15-N3 L-histidine, 25.3% sodium chloride, 0.133% polysorbate 80, 66.7% trehalose. Fig. S1 shows an image of lyophilized HPV VLP prepared at three different starting solution pH.

Solid-State NMR Spectroscopy

Solid-state NMR experiments were carried out on an Avance III 500 spectrometer (11.7 T) equipped with a 4-mm triple-resonance H/X/Y probe (tuned to $^{1}H/^{13}C/^{15}N$) in the Biopharmaceutical NMR Laboratory (BNL), Pharmaceutical Sciences (Merck & Co. Inc, West Point, PA 19486, United States). 1D ^{13}C and ^{15}N spectra of samples were acquired at a MAS frequency of 12 kHz and at room temperature. A typical ^{1}H 90° pulse radio-frequency (RF) power was 83 kHz. During cross polarization (CP) period from ^{1}H to ^{13}C or ^{15}N, RF power on ^{1}H and X (^{13}C or ^{15}N) channels were matched to Hartmann-Hahn conditions, and a linear gradient pulse from 90% to 100% was used to on ^{1}H channel to enhance the transfer efficiency. A CP contact time of 2 ms and 2.5 ms was used for ^{1}H–^{13}C and ^{1}H–^{15}N transfers, respectively. During ^{13}C and ^{15}N acquisition, the ^{1}H RF power of the SPINAL decoupling scheme was set to 83 kHz. A recycle delay of 2 s was used for all the 1D experiments. 2 k-6 k scans were commonly acquired for 1D spectra resulting in experimental times of 1–5 h.

2D $^{13}C-^{13}C$ COmbined $R2^{v}_{n}$-Driven (CORD)[43] homonuclear correlation experiments were acquired with a CORD mixing time of 50 ms. A typical 2D CORD took 10 h−31 h with a recycle delay of 1.5 s and 64 to 196 scans. 2D $^{15}N-^{13}C$ double CP (DCP) experiments were obtained with a $^{1}H-^{15}N$ contact time of 2 ms and a $^{15}N-^{13}C$ contact time of 8 ms. A ^{13}C 90° pulse was 4.8 us. With 521−2048 scans, and 8 points in indirect dimension and a recycle delay of 8 s, the experimental time for a DCP spectrum was approximately 9−36 h. For crystalline histidine, 2D $^{1}H-^{13}C$ heteronuclear correlation (HETCOR) spectrum was obtained with 50 μs CP contact time. 32 scans were repeatedly accumulated with a recycle delay of 2s. With an acquisition of 512 points in the indirect ^{1}H dimension, a total experiment time was approximately 9 h 2D $^{1}H-^{15}N$ HETCOR spectrum with a contact time of 50 μs was acquired with 512 points in the ^{1}H dimension and 32 consecutive scans per point resulting in an experimental time of approximately 9 h, All spectra were processed in Bruker TopSpin. 1D spectra were obtained by zero filling, application of Gaussian function and Fourier transformation. Gaussian or Qsine window functions were applied for 2D spectra. ^{13}C chemical shifts are referenced to alpha-glycine carbonyl peak at 176.5 ppm and ^{15}N chemical shifts were reference to glycine nitrogen at 33.4 ppm. ^{1}H chemical shifts were externally referenced to water at 4.70 ppm.

Results

This study aims to establish a protocol to probe microenvironmental acidity by utilizing the chemical shifts of histidine as a probe molecule. We firstly explored the chemical shift changes of histidine lyophilized at various pH values, then established the pH-dependency, and finally utilized the protocol to examine the solid-state pH of lyophilized vaccine and protein formulations. 1D and 2D homo- and heteronuclear correlations in combination with ^{13}C and ^{15}N isotopically labeling strategy were utilized.

Spectroscopic Characterization of Lyophilized Histidine in the Amorphous Form

1D ^{13}C and ^{15}N spectra of ^{13}C and ^{15}N isotopically enriched histidine in a lyophilized formulation in comparison with those of a crystalline form as received are shown in Fig. 2. ^{13}C and ^{15}N isotopically labeling significantly improves the ssNMR sensitivity and allows for acquiring multinuclear correlation spectra for chemical shift assignments. Spectra of natural abundance histidine in lyophilized formulations are shown in Fig. S2, which show partial signal overlapping with trehalose. Crystallization of histidine is not observed in the ssNMR spectra, as indicated by the broad ^{13}C and ^{15}N peaks. The amorphous nature is also confirmed by the broad PXRD patterns in Fig. S4. The ssNMR signals of histidine in the lyophilized sample prepared from 20 mM sodium phosphate buffer with 5 w/v % trehalose and pH 7 are significantly broadened showing linewidth of approximately 6.6 ppm and 8.5 ppm for ^{13}C and ^{15}N, respectively (Fig. 2). As a comparison, the corresponding ^{13}C and ^{15}N linewidth is approximately 1.2 ppm respectively for the crystalline form. The broad spectra identify the amorphous nature of lyophilized powder. For histidine crystallized near neutral pH, coexistence of tautomeric states of histidine including a neutral τ tautomer and a cationic form was identified given the high-resolution spectra commonly obtained for crystalline samples.[35] However, due to significant line broadening, one set of carbon and nitrogen peaks is identified for the amorphous form, which corresponds to averaged chemical shifts of different protonation states and tautomers at equilibrium. It will be interesting to gain insights into the protonation and tautomeric state of amorphous histidine obtained upon lyophilization. We therefore performed chemical shift assignments by referencing to existing literatures and following a protocol established previously.[35,44]

We acquired 2D $^{13}C-^{13}C$, $^{13}C-^{15}N$, $^{1}H-^{13}C$, and $^{1}H-^{15}N$ correlation spectra in addition to 1D spectra for unambiguous resonance assignments of amorphous histidine lyophilized from the solution samples prepared at pH 4.5 to 11.0. Fig. 3 illustrates an example of peak assignments of amorphous histidine using 1D and 2D spectra at pH 6. The same experimental protocol was utilized to assign resonances of crystalline histidine (Fig. S3) which allows the identification of neutral τ tautomer as the main form in the sample.

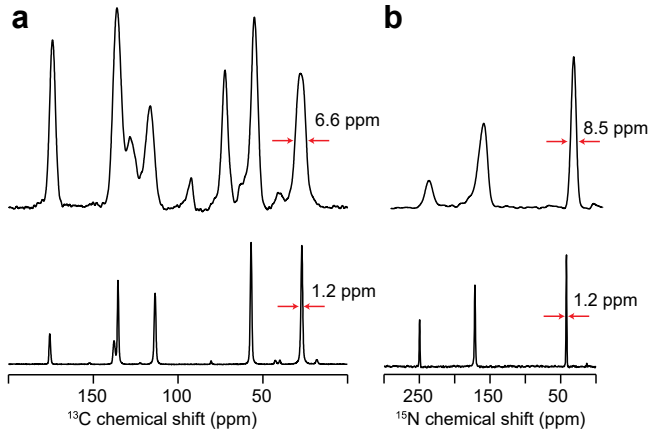

Fig. 2. Comparison of 1D^{13}C (a) and ^{15}N spectra (b) of ^{13}C and ^{15}N isotopically labeled crystalline histidine (bottom) and amorphous histidine (top) in a lyophilized formulation prepared from aqueous solution of 20 mM sodium phosphate buffer with 5 w/v % trehalose and at pH 7.0. Histidine, trehalose, sodium phosphate account for 5.9%, 89.1% and 5% w/w of the lyophilized product, respectively. Full width at half maximum (FWHM) of a few representative peaks is shown in ppm.

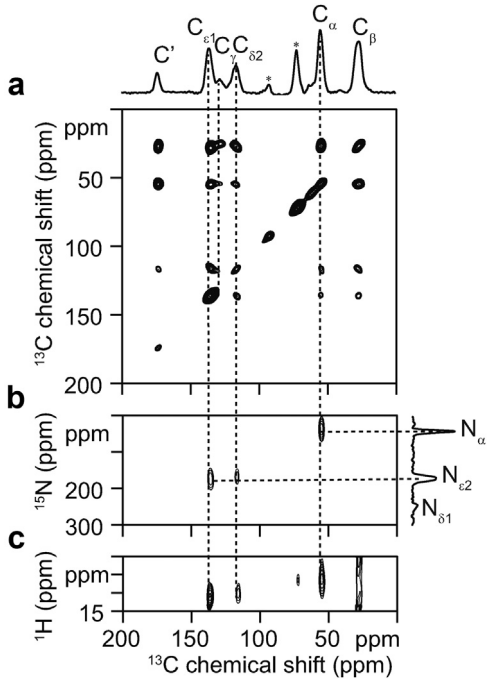

Fig. 3. Representative chemical shift assignments of amorphous histidine lyophilized from a solution containing 5 w/v % trehalose at pH 6 using 2D $^{13}C-^{13}C$ homonuclear (a), $^{13}C-^{15}N$ (b) and $^{1}H-^{13}C$ (c) heteronuclear correlations. 1D ^{13}C and ^{15}N spectra are displayed along the axis. Signals from unlabeled trehalose in 1D ^{13}C spectrum is marked with asterisk. Histidine and trehalose account for 6% and 94% w/w of the final lyophilized product, respectively.

The ^{1}H, ^{15}N and ^{13}C chemical shifts are summarized in Table S1. 2D spectra establish correlations among proton, carbon, and nitrogen spins for unambiguous chemical shift assignments of ^{13}C and ^{15}N. For example, C_γ is not directly bonded to $N_{\varepsilon 2}$ and therefore can be assigned to the peak without a cross peak to $N_{\varepsilon 2}$ in the 2D $^{15}N-^{13}C$ spectrum. The knowledge of chemical shifts enables to identify the dominant form in an amorphous mixture. At pH 6.0, $N_{\delta 1}$ has a chemical shift of approximately 246.6 ppm suggesting a deprotonated $N_{\delta 1}$. $C_{\delta 2}$ shows a shift of 118.1 ppm, lying in between that of a cationic form and a neutral τ tautomer. Therefore, the lyophilization process retains a mixture of cationic and neutral histidine which coexist in the starting solution of pH. At pH 4.5, $N_{\delta 1}$ and $N_{\varepsilon 1}$ exhibit one broad peak at 175.4 ppm, agreeing with a protonated imidazole ring of a cationic histidine. At pH 7.0 and 8.0, the coexistence of a cationic form and a neutral τ tautomer remains with the neutral form becoming dominant. At pH 11.0, the carbonyl carbon shows a chemical shift at 181.7 ppm and $C_{\delta 2}$ has a chemical shift at 115.1 ppm, suggesting an anionic τ tautomer. It should be noted that the presence of π tautomer is possible at pH 11.0 but couldn't be assigned due to peak overlapping. Li and Hong reported the absence of the neutral τ tautomer of crystalline histidine at pH 8.5 due to its instability.[35] At pH 11.0, the coexistence of the anionic π and τ tautomers was identified and it caused linebroadening,[35] which is also observed in our spectra. The metastable anionic π tautomer is reported to convert to τ tautomer when the dry sample is hydrated.[35] It has been noted that a $C_{\delta 2}$ chemical shift at > 122 ppm is suggestive of a predominant π tautomer.[45] ^{1}H peaks in the indirect dimension of the 2D spectra are broad (Fig. 3C), as expected, due to strong proton-proton dipolar couplings in the solids and disordered nature of the amorphous materials.

Protonation States and Chemical Shift Dependence of Histidine in Lyophilized Matrix

Stacked 1D ^{13}C and ^{15}N spectra of histidine acquired at pH 4.5 to 11 are displayed in Fig. 4A and B showing the imidazole carbons and nitrogen. Generally, similar linewidth and peak pattern are consistently observed in 1D ^{13}C and ^{15}N spectra in the pH range under our investigation. Interestingly, chemical shift perturbations are observed at different pH conditions. Dashed lines mark the shifting of ring carbons and nitrogen in 1D spectra. The correlation between pH values of the starting solution and ^{13}C and ^{15}N chemical shifts of histidine imidazole ring in the lyophilized samples are plotted in Fig. 4C. Chemical shifts of histidine imidazole ring demonstrate a systematic shift with increasing pH values. C_ε shows a downfield shift, with an average shift of 0.30 ppm per pH unit. C_γ, $C_{\delta 2}$ and $N_{\varepsilon 2}$ show an upfield shift from pH 4.5 to 11.0, and the average shift per unit is 0.49 ppm, 0.52, and 1.35 ppm, respectively. Since nitrogen atoms are directly involved in protonation and deprotonation, nitrogen chemical shifts are shown to be more sensitive to pH changes. $C_{\delta 2}$ chemical shift is most sensitive to pH change in the acidic range with a shift of 0.4 ppm from pH 4.5 to pH 6.0. Near physiological pH, a pH unit change causes an average shift of 0.43, 0.8, 0.77 and 2.5 ppm for C_ε, C_γ, $C_{\delta 2}$, and $N_{\varepsilon 2}$, respectively, showing more sensitivity than the larger pH range from 4.5 to 11.0. These pH-dependent changes suggest that the change of histidine chemical shifts can be utilized to probe the microenvironmental acidity in lyophilized solids.

Samples in Fig. 4 was prepared from solutions containing 20 mM sodium phosphate buffer. The formulation pH is often maintained by utilizing a buffer system that covers the range of the desired pH and has reasonable buffer capacity. To evaluate the capability by utilizing histidine as the only buffer agent, we prepared the lyophilized histidine samples without sodium phosphate buffer. Chemical shift assignments of samples containing 20 mM

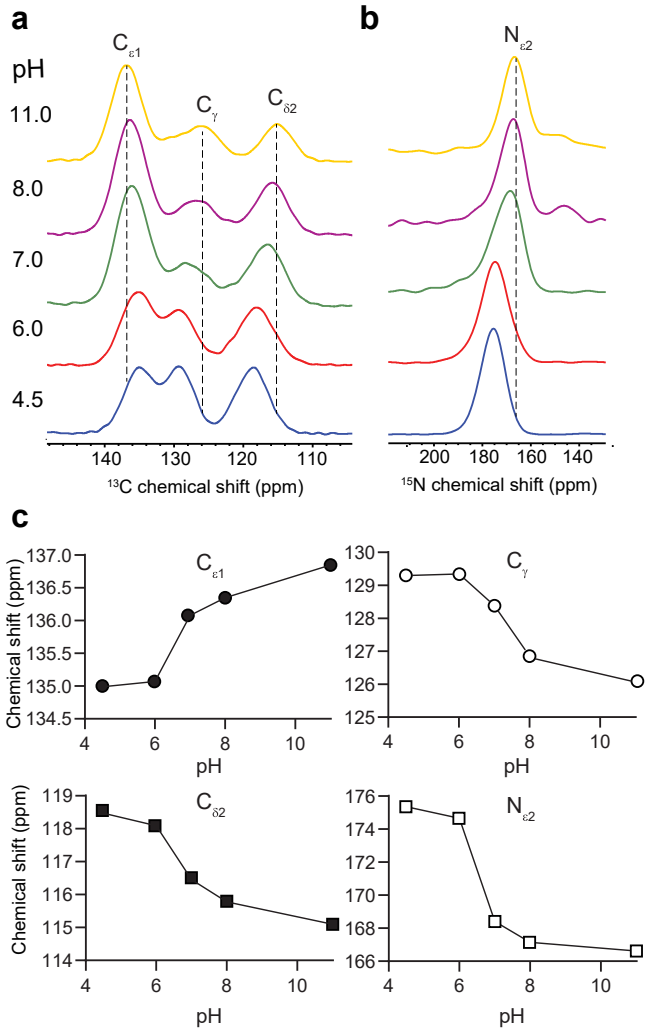

Fig. 4. 1D ^{13}C (a) and ^{15}N (b) spectra of ^{13}C and ^{15}N labeled histidine/trehalose/sodium phosphate lyophilized powder at pH 4.5 to 11.0. (c) Correlation between C_ε, C_γ, $C_{\delta 2}$ and $N_{\varepsilon 2}$ chemical shifts of amorphous histidine and pH values at which the formulations were prepared. Histidine, trehalose, sodium phosphate account for 5.9%, 89.1% and 5% w/w of final lyophilized products, respectively.

histidine and 5 w/v% trehalose are summarized in Table S1. Fig. S5 shows correlations of histidine chemical shifts and pre-lyo solution pH in the absence of sodium phosphate. Similar trend of chemical shift changes with pH increases is observed as those in Fig. 4. To evaluate the impact on chemical shift of histidine with and without sodium phosphate buffer, the comparisons are shown in Fig. 5A–E. The data have shown that 20 mM sodium phosphate buffer has minor impact on histidine chemical shifts at different pH values with correlation coefficient values of approximately 0.97. One exception is observed at pH 6.0 with a relatively smaller correlation coefficient of approximately 0.91. Without sodium phosphate buffer, $N_{\varepsilon 2}$ peak at 168.9 ppm is significantly broader than that at 174.6 ppm with the presence of sodium phosphate buffer (Fig. 6A). A higher $N_{\varepsilon 2}$ chemical shift corresponds to an equilibrium towards the cationic form.[35] Compared to signals of crystalline cationic and neutral forms (Fig. 1), the linewidth of amorphous histidine is much broader representing an averaged distribution of the two forms. Similarly, ^{13}C spectra show a distribution of different forms as shown in Fig. 6B. The peaks at 135.1 and 136.0 ppm assigned to $C_{\varepsilon 1}$ reflects averaged signals of $C_{\varepsilon 1}$ of the charged and neutral forms and C_γ of the neutral form. Therefore, the presence of sodium

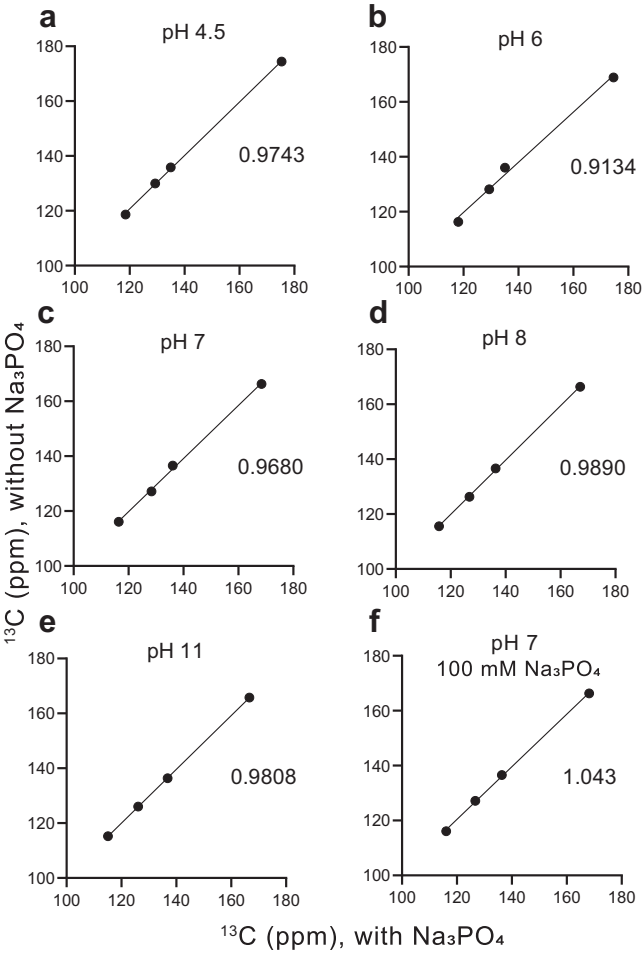

Fig. 5. Correlation of C_ε, C_γ, $C_{\delta 2}$, and $N_{\varepsilon 2}$ chemical shifts of histidine with (x-axis) and without (y-axis) sodium phosphate buffer in lyophilized His/trehalose prepared at different pH. (a–e): 20 mM sodium phosphate buffer at pH 4.5 to 11, in which histidine, trehalose, and sodium phosphate account for 5.9% 89.1% and 5% w/w of the final lyophilized product, respectively. (f): 100 mM sodium phosphate buffer at pH 7 ± 0.5. The composition of histidine, trehalose, and sodium phosphate is 4.2%, 64.7% and 31.1% w/w, respectively. Slopes of the linear correlation prediction are reported in the plots.

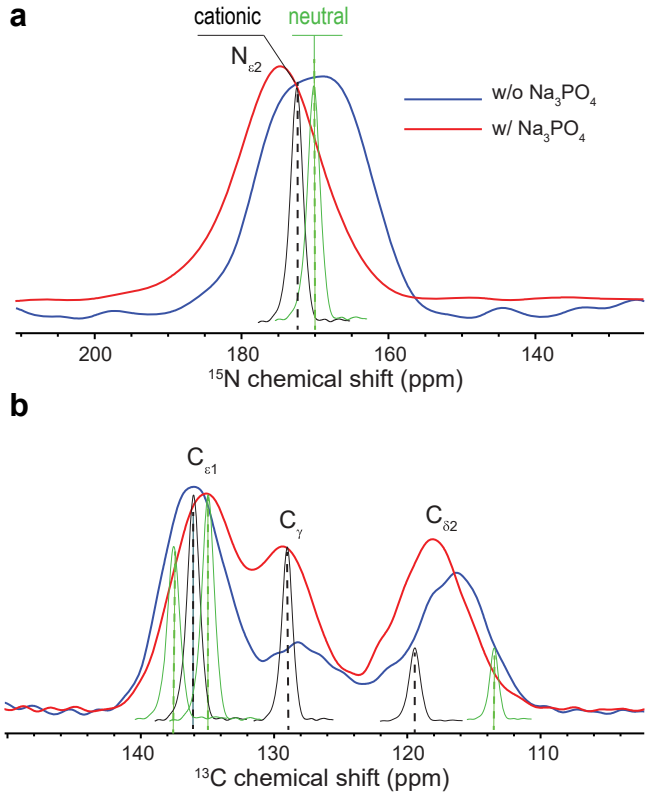

Fig. 6. Comparison of 1D ^{15}N (a) and ^{13}C (b) spectra of ^{13}C and ^{15}N-labeled histidine/trehalose formulations prepared at an aqueous solution pH of 6, with (red) and without (blue) sodium phosphate. Simulated spectra of cationic (black) and neutral (green) states of crystalline histidine at the chemical shifts reported previously.[35] Histidine and trehalose account for 6% and 94% w/w of the final lyophilized product, respectively.

phosphate favors the protonated imidazole, whereas the absence of buffer results in a broader distribution of the cationic and neutral states, suggesting a slightly stronger acidity.

It is well known that pH shifts can occur during freezing due to selective crystallization of basic component of the sodium phosphate buffer.[11,14] We therefore compare the impact of 100 mM sodium phosphate on pH during lyophilization. Fig. 5F shows a correlation of C_ε, C_γ, $C_{\delta 2}$, and $N_{\varepsilon 2}$ chemical shifts for amorphous histidine prepared with and without 100 mM sodium phosphate. A good linear correlation coefficient of 1.043 is obtained for C_ε, C_γ, $C_{\delta 2}$, and $N_{\varepsilon 2}$ chemical shifts. Absolute chemical shift differences of 0.21, 0.44, 0.01, and 1.85 ppm are recorded for C_ε, C_γ, $C_{\delta 2}$, and $N_{\varepsilon 2}$, which suggest a pH change within one unit. However, a pH change of 4.1 units of 100 mM sodium phosphate buffer has been reported due to salt crystallization when cooled from room temperature to −25 °C.[11] One hypothesis is that the presence of 5 w/v % trehalose prevents salt crystallization under our experimental conditions. A reduced pH shift of 0.2 unit has been reported for 100 mM phosphate buffer with 5 w/v % cellobiose.[11] Moreover, it has been reported that 5 w/v % trehalose can completely inhibit salt crystallization of sodium phosphate buffer and decrease the magnitude of pH shift by 1.7 units.[14] It should be noted that the inhibitory effect of solutes on sugar or salt crystallization depends on experimental factors such as sample geometry and cooling rate.[46] The formulation composition also plays a role in the inhibitory effect on recrystallization, including sugar and salt concentration, initial pH, and presence of other excipients.[10,46]

Histidine as A Molecular Probe of Acidy in Lyophilized Vaccine and Protein Formulations

Histidine is a commonly used buffer and stabilizer in vaccine and protein formulations, and therefore an internal sensor for probing pH changes during processing, shipment, and storage. To demonstrate the feasibility of using histidine to probe pH changes in vaccine formulations, we prepared three lyophilized HPV formulations at pH 4.5, 6.0 and 8.0, with 20 mM labeled histidine, 5 w/v % trehalose and 10 mM unlabeled histidine in the starting solution. 1D ^{13}C and ^{15}N spectra of histidine in these samples can be obtained at approximately 2 h. Fig. 7A shows the spectral area of imidazole ring carbons, as an example. Interestingly, histidine spectra of the HPV formulation show similar spectral features, i.e., peak positions and linewidth, as the vaccine-free samples in Fig. 4A. 2D ^{13}C–^{13}C and ^{15}N–^{13}C spectra (data not shown) are further utilized to refine the resonance assignments. Chemical shift perturbations can be readily observed from pH 4.5 to 8.0 in 1D and 2D spectra in Fig. 7A and B. The average shift of $C_{\varepsilon 1}$, C_γ, $C_{\delta 2}$, and $N_{\varepsilon 2}$ per pH unit is 0.44, 0.63, 0.79, and 2.44 ppm, respectively. The chemical shifts of histidine agree well with those of reference samples without HPV (Fig. 4A), showing a linear correlation coefficient of nearly 1.0 at all three pH conditions displayed in Fig. S6A–C. This

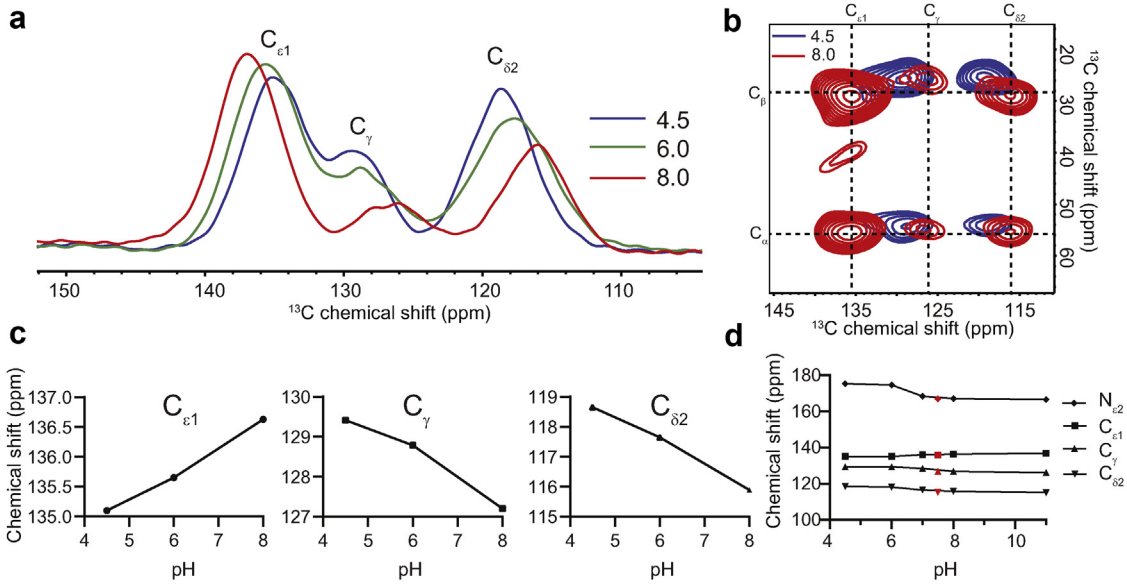

Fig. 7. Microenvironmental acidity of lyophilized formulations of HPV (a–c) and LDH (d) probed by chemical shift changes of histidine. Chemical shift changes of histidine in HPV vaccine formulations lyophilized at different pH conditions (pH 4.5, 6.0 and 8.0) observed in 1D ^{13}C ssNMR spectra (a) and 2D ^{13}C–^{13}C spectra (b) of HPV vaccine formulations; (c) Correlations between ^{13}C and ^{15}N chemical shifts and pH values. (d) Plot of $C_{\varepsilon1}$, C_{γ}, $C_{\delta2}$, and $N_{\varepsilon2}$ chemical shifts of histidine in LDH formulation as a function of the starting pH (red) with reference to standard samples without the protein (black). The lyophilized LDH product contains 0.01% w/w LDH, 4.24% w/w histidine, 64.69% w/w trehalose, and 31.10% w/w sodium phosphate. The relative ratio of histidine to phosphate is 1:5. The weight composition of the lyophilized HPV33 cakes were 0.721% HPV33 VLPs, 2.07% L-histidine, 5.00% $^{13}C_6$, $^{15}N_3$ L-histidine, 25.3% sodium chloride, 0.133% polysorbate 80, and 66.7% trehalose.

indicates that biomacromolecular components in HPV vaccine does not impact the acidity in the lyophilized formulations at given conditions. We also tested the protocol on a lactate dehydrogenase (LDH) protein formulation prepared from a starting solution with 10 μg/mL protein, 5% trehalose, and 20 mM labeled histidine at pH 7.5. Fig. 7D shows the $C_{\varepsilon1}$, C_{γ}, $C_{\delta2}$, and $N_{\varepsilon2}$ chemical shift agree well with the trend of chemical shift and pH previously established in Fig. 4C. In a plot correlating chemical shifts of histidine with and without LDH shown in Fig. S6D, one significant chemical shift change is observed for $N_{\varepsilon2}$ nitrogen showing a difference of 1.2 ppm in Fig. S7. As shown in Fig. S7, all ^{13}C peaks overlay well between the samples with and without the protein, suggesting the stability of solid acidity. Therefore, the observation of chemical shift change of $N_{\varepsilon2}$ might indicate histidine-protein interaction. Multiple possible interactions of histidine and protein sites have been reported previously, including π- π and hydrogen- π interactions with aromatic residues and cationic- π interactions in which the histidine can act as both the cation role and the aromatic π-motif depending on the pH.[47] Hydrogen bonding between stabilizing carbohydrates with dried proteins was shown to be important for stabilizing freeze-dried proteins.[48,49]

Discussion

Biologics are often buffered and stored in frozen or lyophilized state. Undesired pH changes can occur during freezing step in freeze-drying potentially resulting in the instability of macromolecules in the final lyophile. The pH shifts in frozen aqueous solution have been well documented in previous studies. For example, Suryanarayanan and coworkers investigated pH shifts in protein formulations upon freezing by utilizing a low temperature electrode.[9,11,14,30] This enabled investigation of protein aggregation[11] and salt disproportionation[44] caused by pH shift upon cooling to −25 °C. The detection of pH shift in frozen solutions using the same technique also enabled the study of inhibition effect of trehalose and mannitol on pH shift in PBS buffer.[14] In addition, pH shifts of 0.7–1.9 units for frozen solutions of 200 mM histidine buffer solution prepared at pH 5.0 to 7.0 have been observed using a low-temperature pH meter.[30] In a study to investigate the effect of buffer and stabilizer on the stability of LDH during freezing, Al-Hussein et al. detected pH changes in the formulations by adding an universal pH indicator to the formulations prior to freezing.[32] However, to our knowledge, an non-invasive method to probe pH of freeze-dried pharmaceutical solids is not yet available prohibiting detailed quality assessment of drug products. pH measurement of solids is not applicable by electrodes or universal pH solution due to the absence of hydrogen cations solvated in solution.

The NMR-based chemical shift approach to determine pH of solution relies on the presence of fast chemical exchange between acid (HL, a proton donor) and base (L, a proton acceptor) forms of indicator species and thus a single chemical shift is observed. The observed chemical shift (δ^{obs}) is the weighted average of the two forms at equilibrium:

$$\delta^{obs} = \chi_{HL}\delta_{HL} + \chi_{L}\delta_{L} \quad (1)$$

where δ_{HL} and δ_{L} are the limiting chemical shifts of the acid and base forms, respectively, and weighting factors χ_{HL} and χ_{L} are the corresponding molar factions. For an monoprotic base with known protonation constant K and limiting chemical shifts δ_{HL} and δ_{L}, the pH is defined by a Henderson-Hasselbalch type expression and can be calculated from the observed chemical shift (δ^{obs}) using the following equation[50]:

$$\mathrm{pH} = \log K + \log\frac{\delta^{obs} - \delta_{HL}}{\delta_{L} - \delta^{obs}} \quad (2)$$

Equation (2) is the principle of determining solution pH using monoprotic base with at least one NMR active nucleus as a pH indicator. The capacity of NMR spectroscopy to monitor in situ and ex situ pH changes has been demonstrated for a variety of indicators by observing ^{1}H, ^{13}C, ^{15}N, ^{19}F, and ^{31}P.[50–58] By performing a titration

curve of the chemical shift as a function of pH in the exact buffer conditions, one can establish the equivalence between proton chemical shift of ionizable compounds and the pH value.[59,60] ^{13}C magnetic resonance imaging and dynamic nuclear polarization technique have been used for measuring *in vivo* tissue pH by determining the ratio of hyperpolarized bicarbonate ($H^{13}CO_3^-$) and CO_2 following intravenous injection of hyperpolarized bicarbonate.[53] ^{31}P magnetic resonance spectra have also been utilized to calculate extracellular pH of tumors.[61] Simultaneous detection of ^{1}H and ^{31}P spectra allows monitoring of pH calculated from the measured chemical shifts during chemical reaction and enzyme catalysis.[62] Several series of organic compounds of known basicity whose carbon-bound protons chemical shifts respond to pH changes have been published as pH indicators in NMR-based determination of pH.[50,54–57]

Equations (1) and (2) suggest the chemical shift dependence on pH values. Histidine is an ideal pH indicator due to the presence of four protonation sites. The proton chemical shift of histidine shows a high sensitivity on probing pH changes of pH and salt concentration in solution.[59] With a pK of 7.22, imidazole ring has been commonly utilized as a pH indicator in the range of 5.5–8.9.[50,56] Chemical shift changes of successive deprotonation states have been identified in the solid state showing potential as a pH indicator in crystalline and lyophilized solids.[35,39] Generally, the relatively sharp and broad peaks in crystalline and lyophilized samples represent highly ordered structure and conformational inhomogeneity, respectively (Fig. 2). Histidine samples prepared from crystallization showed well-resolved peaks allowing the identification of the cationic and neutral forms.[33] As illustrated by the peaks in the dotted line in Fig. 6, for example, cationic and neutral forms respectively give $C_{\delta 2}$ chemical shifts at 113.6 and 119.4 ppm, and $N_{\varepsilon 2}$ chemical shifts at 176.3 and 171.1 ppm. However, at pH 6.0, a value equal to a pKa, the broad peaks of amorphous histidine samples cover the chemical shifts of both cationic and neutral forms (blue and red spectra in Fig. 6), exhibiting a distribution of protonation states. For example, the broad peaks of $C_{\delta 2}$ in amorphous histidine centered at 118.1 and 116.3 ppm with and without sodium phosphate (Fig. 6B), respectively. Interestingly, amorphous histidine in lyophilized formulations without sodium phosphate exhibit an even broader peak of $N_{\varepsilon 2}$ at 168.9 ppm in the blue spectrum in Fig. 6A, which covers a range of chemical shifts representing cationic and neutral states. In contrast, the $N_{\varepsilon 2}$ peak of the sample with sodium phosphate in the red spectrum in Fig. 6A centered at 174.6 ppm, suggesting the cationic state is more dominating than that without phosphate buffer. This comparison suggests that the utilization of sodium phosphate helps to maintain the protonated state of histidine near pKa, and thus the probed acidity, in the amorphous matrix.

Deprotonation of the imidazole ring induced by an increasing pH causes charge redistribution and electric deshielding changes, which explains the pH dependence of chemical shifts. However, different carbon and nitrogen atoms of the imidazole ring vary in the sensitivity and capacity when responding to pH changes. In crystalline histidine,[33] $C_{\delta 2}$ and $N_{\varepsilon 2}$ showed monotonical shifts from the cationic form to the ionic state with a shift of 5.8 ppm and 9 ppm, respectively. Changes of $C_{\varepsilon 1}$ chemical shift were within 1 ppm upon two-step deprotonation from pH 4.5 to 11. The deprotonation of $N_{\delta 1}$ also caused a significant downfield shift of C_γ from 128.7 ppm in the cationic form to 137 ppm in the neutral form. C_γ of the anionic τ tautomer has a chemical shift similar to that of the neutral state. In our study, consistent with the crystalline form, monotonical shifts of $C_{\delta 2}$ and $N_{\varepsilon 2}$ are also identified in amorphous histidine from pH 4.5 to 11 upon deprotonation of $N_{\delta 1}$ of the imidazole ring and the amino end. The absolute chemical shift changes for $C_{\delta 2}$ and $N_{\varepsilon 2}$ were 3.4 ppm and 8.8 ppm, respectively. Due to the overlapping of C_γ signal with $C_{\varepsilon 1}$ in amorphous histidine at pH 6 and above, the observed peak shifting of $C_{\varepsilon 1}$ is partially attributed to the shifting of C_γ. The downfield shifts of C_γ result from a combined effect of deprotonation and tautomerization of the imidazole ring. Taken together, our results suggest chemical shifts of $C_{\delta 2}$ and $N_{\varepsilon 2}$ of histidine are good candidates for probing the change of microenvironmental acidity in amorphous formulations since their peaks are resolved and show monotonical shifts in a wide range.

Delpuech and co-workers show that acid dissociation constants of pKa_i measured in lyophilized histidine can be calculated from the acid-to-base molar ratio (r) in the lyophilizate and the pH of the parent solution.[39] Using ^{13}C solid state NMR, they determined that pKa values of the three consecutive deprotonation processes are very close to those reported in solution. It was therefore indicated that a conventional pH in solution can be assigned to the lyophilized powder, which corresponds to the pH measured in the parent liquid under the same ionic strength and temperature. In contrast to our study, their lyophilized histidine exhibited remarkable spectral resolution in which the base and acid forms at each pH were well resolved, allowing for chemical shift assignments of each form. Such narrow linewidth of ssNMR spectra might indicate several histidine samples lyophilized from solutions were in crystalline form instead of amorphous form in their study. In contrast, the goal of our study is to evaluate the protonation states of amorphous histidine samples. We show that a combination of 5 w/v% trehalose and 20 mM histidine in the formulation is an effective method to prevent histidine and buffer crystallization (Fig. 2A), making it possible to evaluate the pH-dependence of chemical shifts of histidine in the amorphous form. We show that ^{13}C and ^{15}N chemical shifts of amorphous histidine are sensitive indicators of solid-state pH. In the formulation solution, pH affects the equilibrium of histidine protonation and tautomerization states which have distinct chemical shifts. Due to an equilibrium of different forms in dry state, the change of amorphous histidine chemical shifts is shown to well correlate with solid state pH (Fig. 4). In addition, the maintenance of the amorphous state of histidine has been shown to be important for its stabilizing effect in freeze-dried protein formulations.[32] We then further demonstrate the incorporation of histidine into protein and vaccine formulations as a promising approach for monitoring microenvironmental pH of solid-state protein drug products (Fig. 7). The ^{13}C and ^{15}N isotopically labeled histidine utilized in this study significantly improves the ssNMR sensitivity by approximate 90 and 270 folds, respectively, considering the natural abundance of ^{13}C (1.1%) and ^{15}N (0.37%). Natural abundance histidine in formulations produced in the industrial practice can also be readily used to indicate pH changes in lyophiles as shown in Fig. S2, with the price of a longer acquisition time. Moreover, ^{1}H represents the most NMR-sensitive nuclei and particularly useful to probe the change of acidity. However, ^{1}H spectra at moderate spinning frequencies, e.g.,12 kHz, cannot offer the resolution to unambiguously identify the protonation states. Recent advances on ultrafast magic angle spinning significantly narrow the proton linewidth by averaging the spin interactions and can be utilized to obtain accurate ^{1}H chemical shifts of crystalline and amorphous solids in future studies.[63–65]

Since the change in formulation pH can affect stability of biologics and result in protein denaturation, we expect this method can be used to not only measure pH changes in biologic solids but also provide an indicator of potential instability. Further studies will focus on the correlation between histidine chemical shift changes and protein stability. Lyophilized pharmaceutical formulations usually show significant line broadening of NMR signals as shown in our study, which prevent identification of different protonation states of histidine and thus quantitative determination of

pH. Recent progress of ultrafast MAS (UF-MAS) significantly narrows proton spectral linewidth and enables proton detection at a high resolution.[63–68] The application of ^{1}H detection at UF-MAS can provide the spectral resolution and sensitivity to observe imidazole protons for identifying different histidine protonation states, without the need of isotopic enrichment.

Conclusions

Microenvironmental acidity of solid-state protein formulation can shift during the freezing and drying process in lyophilization, resulting in instability of drug substances and products. We developed a ssNMR spectroscopic protocol to probe microenvironmental pH of lyophilized biological products in a non-invasive manner by detecting the chemical shift changes of histidine. The incorporation of ^{13}C, ^{15}N isotopically labeled histidine, a common buffer or stabilizer, in the formulation enables fast acquisition of 1D and 2D ssNMR spectra for chemical shift assignments of amorphous histidine. ^{13}C and ^{15}N chemical shifts of amorphous histidine are shown to well correlate with the pH of solutions the lyophilized powder was prepared from, and therefore can be used to probe pH changes in lyophilized samples. With (5 w/v%) trehalose in the formulation, the different capacity of sodium phosphate buffer showed minor impact on solid state pH. Furthermore, a pH dependent chemical shift change of histidine is established in model vaccine and protein formulations. This work provides likely the first documented case to probe pH of lyophilized biologics using histidine as a molecular probe. In future work, we expect to further develop this method to probe the impact of buffer, protein, and other excipients on pH shift in freeze-dried samples and its correlation with formulation stability.

Acknowledgements

M. L. and X. L. are grateful to MRL postdoctoral research program. The authors thank Drs. Yoen-Ju Son, Ashley Lay-Fortenbery, Ashish Punia, and Jing Ling for their scientific discussions.

Appendix A. Supplementary Data

Supplementary data to this article can be found online at https://doi.org/10.1016/j.xphs.2020.11.017.

References

1. Chang LL, Pikal MJ. Mechanisms of protein stabilization in the solid state. *J Pharm Sci*. 2009;98(9):2886-2908.
2. Authelin JR, Rodrigues MA, Tchessalov S, et al. Freezing of biologicals revisited: scale, stability, excipients, and degradation stresses. *J Pharm Sci*. 2020;109(1):44-61.
3. Zbacnik TJ, Holcomb RE, Katayama DS, et al. Role of buffers in protein formulations. *J Pharm Sci*. 2017;106(3):713-733.
4. Krauskova L, Prochazkova J, Klaskova M, et al. Suppression of protein inactivation during freezing by minimizing pH changes using ionic cryoprotectants. *Int J Pharm*. 2016;509(1-2):41-49.
5. Roessl U, Humi S, Leitgeb S, Nidetzky B. Design of experiments reveals critical parameters for pilot-scale freeze-and-thaw processing of L-lactic dehydrogenase. *Biotechnol J*. 2015;10(9):1390-1399.
6. Cao E, Chen Y, Cui Z, Foster PR. Effect of freezing and thawing rates on denaturation of proteins in aqueous solutions. *Biotechnol Bioeng*. 2003;82(6):684-690.
7. Pikal-Cleland KA, Carpenter JF. Lyophilization-induced protein denaturation in phosphate buffer systems: monomeric and tetrameric beta-galactosidase. *J Pharm Sci*. 2001;90(9):1255-1268.
8. Pikal-Cleland KA, Rodriguez-Hornedo N, Amidon GL, Carpenter JF. Protein denaturation during freezing and thawing in phosphate buffer systems: monomeric and tetrameric beta-galactosidase. *Arch Biochem Biophys*. 2000;384(2):398-406.
9. Koranne S, Thakral S, Suryanarayanan R. Effect of formulation and process parameters on the disproportionation of indomethacin sodium in buffered lyophilized formulations. *Pharm Res (N Y)*. 2018;35(1):21.
10. Gomez G, Pikal MJ, Rodriguez-Hornedo N. Effect of initial buffer composition on pH changes during far-from-equilibrium freezing of sodium phosphate buffer solutions. *Pharm Res*. 2001;18(1):90-97.
11. Thorat AA, Munjal B, Geders TW, Suryanarayanan R. Freezing-induced protein aggregation - role of pH shift and potential mitigation strategies. *J Control Release*. 2020;323:591-599.
12. Roessl U, Humi S, Leitgeb S, Nidetzky B. Design of experiments reveals critical parameters for pilot-scale freeze-and-thaw processing of L-lactic dehydrogenase. *Biotechnol J*. 2015;10(9):1390-1399.
13. Anchordoquy TJ, Carpenter JF. Polymers protect lactate dehydrogenase during freeze-drying by inhibiting dissociation in the frozen state. *Arch Biochem Biophys*. 1996;332(2):231-238.
14. Thorat AA, Suryanarayanan R. Characterization of phosphate buffered saline (PBS) in frozen state and after freeze-drying. *Pharm Res (N Y)*. 2019;36(7):98.
15. Bhambhani A, Blue TJ. Lyophilization strategies for development of a high-concentration monoclonal antibody formulation: benefits and pitfalls. *Am Pharm Rev*. 2010;31–38.
16. Doherty C, York P. Microenvironmental Ph control of drug dissolution. *Int J Pharm*. 1989;50(3):223-232.
17. Zannou EA, Ji Q, Joshi YM, Serajuddin AT. Stabilization of the maleate salt of a basic drug by adjustment of microenvironmental pH in solid dosage form. *Int J Pharm*. 2007;337(1-2):210-218.
18. Badawy SI, Williams RC, Gilbert DL. Effect of different acids on solid-state stability of an ester prodrug of a IIb/IIIa glycoprotein receptor antagonist. *Pharm Dev Technol*. 1999;4(3):325-331.
19. Siepe S, Lueckel B, Kramer A, Ries A, Gurny R. Strategies for the design of hydrophilic matrix tablets with controlled microenvironmental pH. *Int J Pharm*. 2006;316(1-2):14-20.
20. Tatavarti AS, Hoag SW. Microenvironmental pH modulation based release enhancement of a weakly basic drug from hydrophilic matrices. *J Pharm Sci*. 2006;95(7):1459-1468.
21. Siepe S, Herrmann W, Borchert HH, et al. Microenvironmental pH and microviscosity inside pH-controlled matrix tablets: an EPR imaging study. *J Control Release*. 2006;112(1):72-78.
22. Tran PH, Tran TT, Park JB, Lee BJ. Controlled release systems containing solid dispersions: strategies and mechanisms. *Pharm Res (N Y)*. 2011;28(10):2353-2378.
23. Serajuddin ATM, Jarowski CI. Effect of diffusion layer Ph and solubility on the dissolution rate of pharmaceutical acids and their sodium-salts .2. Salicylic-acid, theophylline, and Benzoic-acid. *J Pharm Sci*. 1985;74(2):148-154.
24. Pudipeddi M, Zannou EA, Vasanthavada M, et al. Measurement of surface pH of pharmaceutical solids: a critical evaluation of indicator dye-sorption method and its comparison with slurry pH method. *J Pharm Sci*. 2008;97(5):1831-1842.
25. Cope SJ, Hibberd S, Whetstone J, MacRae RJ, Melia CD. Measurement and mapping of pH in hydrating pharmaceutical pellets using confocal laser scanning microscopy. *Pharm Res*. 2002;19(10):1554-1563.
26. Tran PHL, Tran HTT, Lee BJ. Modulation of microenvironmental pH and crystallinity of ionizable telmisartan using alkalizers in solid dispersions for controlled release. *J Control Release*. 2008;129(1):59-65.
27. *Gardasil®9: Highlights of Prescribing Information*. Merck Sharp & Dohme Corp; 2014.
28. *Gardasil®: Highlights of Prescribing Information*. Merck Sharp & Dohme Corp; 2006.
29. Chintala R, Bhambhani A. In: Office USPaT, ed. *Human Papillomavirus Vaccine Formulation Comprises Human Papillomavirus-Like Particles Adsorbed onto Aluminum Adjuvant, and Mannitol and Sucrose*. 2014.
30. Sundaramurthi P, Suryanarayanan R. Thermophysical properties of carboxylic and amino acid buffers at subzero temperatures: relevance to frozen state stabilization. *J Phys Chem B*. 2011;115(21):7154-7164.
31. Orii Y, Morita M. Measurement of Ph of frozen buffer solutions by using Ph indicators. *J Biochem*. 1977;81(1):163-168.
32. Al-Hussein A, Gieseler H. Investigation of histidine stabilizing effects on LDH during freeze-drying. *J Pharm Sci*. 2013;102(3):813-826.
33. Costantino HR, Griebenow K, Langer R, Klibanov AM. On the pH memory of lyophilized compounds containing protein functional groups. *Biotechnol Bioeng*. 1997;53(3):345-348.
34. Zbacnik TJ, Holcomb RE, Katayama DS, et al. Role of buffers in protein formulations. *J Pharm Sci*. 2017;106(3):713-733.
35. Li SH, Hong M. Protonation, tautomerization, and rotameric structure of histidine: a comprehensive study by magic-angle-spinning solid-state NMR. *J Am Chem Soc*. 2011;133(5):1534-1544.
36. Blomberg F, Maurer W, Ruterjans H. Nuclear magnetic resonance investigation of 15N-labeled histidine in aqueous solution. *J Am Chem Soc*. 1977;99(25):8149-8159.
37. Platzer G, Okon M, McIntosh LP. pH-dependent random coil H-1, C-13, and N-15 chemical shifts of the ionizable amino acids: a guide for protein pK (a) measurements. *J Biomol NMR*. 2014;60(2-3):109-129.
38. Miao YM, Cross TA, Fu RQ. Differentiation of histidine tautomeric states using N-15 selectively filtered C-13 solid-state NMR spectroscopy. *J Magn Reson*. 2014;245:105-109.
39. Henry B, Tekely P, Delpuech JJ. pH and pK determinations by high-resolution solid-state 13C NMR: acid-base and tautomeric equilibria of lyophilized L-histidine. *J Am Chem Soc*. 2002;124(9):2025-2034.
40. Mensink MA, Nethercott MJ, Hinrichs WLJ, et al. Influence of miscibility of protein-sugar lyophilizates on their storage stability. *AAPS J*. 2016;18(5):1225-1232.

41. Suihko EJ, Forbes RT, Apperley DC. A solid-state NMR study of molecular mobility and phase separation in co-spray-dried protein-sugar particles. *Eur J Pharm Sci*. 2005;25(1):105-112.
42. Lam YH, Bustami R, Phan T, Chan HK, Separovic F. A solid-state NMR study of protein mobility in lyophilized protein-sugar powders. *J Pharm Sci*. 2002;91(4):943-951.
43. Lu X, Guo C, Hou G, Polenova T. Combined zero-quantum and spin-diffusion mixing for efficient homonuclear correlation spectroscopy under fast MAS: broadband recoupling and detection of long-range correlations. *J Biomol NMR*. 2015;61(1):7-20.
44. Lu X, Xu W, Hanada M, Jermain SV, Williams 3rd RO, Su Y. Solid-state NMR analysis of crystalline and amorphous Indomethacin: an experimental protocol for full resonance assignments. *J Pharm Biomed Anal*. 2019;165:47-55.
45. Sudmeier JL, Bradshaw EM, Haddad KEC, et al. Identification of histidine tautomers in proteins by 2D H-1/C-13(delta 2) one-bond correlated NMR. *J Am Chem Soc*. 2003;125(28):8430-8431.
46. Cavatur RK, Vemuri NM, Pyne A, Chrzan Z, Toledo-Velasquez D, Suryanarayanan R. Crystallization behavior of mannitol in frozen aqueous solutions. *Pharm Res (N Y)*. 2002;19(6):894-900.
47. Liao SM, Du QS, Meng JZ, Pang ZW, Huang RB. The multiple roles of histidine in protein interactions. *Chem Cent J*. 2013;7(1):44.
48. Allison SD, Randolph TW, Manning MC, Middleton K, Davis A, Carpenter JF. Effects of drying methods and additives on structure and function of actin: mechanisms of dehydration-induced damage and its inhibition. *Arch Biochem Biophys*. 1998;358(1):171-181.
49. Carpenter JF, Crowe JH. An infrared spectroscopic study of the interactions of carbohydrates with dried proteins. *Biochemistry*. 1989;28(9):3916-3922.
50. Orgovan G, Noszal B. NMR-based determination of pH, free of electrodes and reference compounds. *Anal Chem*. 2018;90(20):12075-12080.
51. Ackerman JJ, Soto GE, Spees WM, Zhu Z, Evelhoch JL. The NMR chemical shift pH measurement revisited: analysis of error and modeling of a pH dependent reference. *Magn Reson Med*. 1996;36(5):674-683.
52. Gerken JB. Measurement of pH by NMR spectroscopy in concentrated aqueous fluoride buffers. *J Fluorine Chem*. 2011;132(1):68-70.
53. Gallagher FA, Kettunen MI, Day SE, et al. Magnetic resonance imaging of pH in vivo using hyperpolarized C-13-labelled bicarbonate. *Nature*. 2008;453(7197):940-U973.
54. Szakacs Z, Hagele G, Tyka R. H-1/P-31 NMR pH indicator series to eliminate the glass electrode in NMR spectroscopic pK(a) determinations. *Anal Chim Acta*. 2004;522(2):247-258.
55. Tynkkynen T, Tiainen M, Soininen P, Laatikainen R. From proton nuclear magnetic resonance spectra to pH. Assessment of H-1 NMR pH indicator compound set for deuterium oxide solutions. *Anal Chim Acta*. 2009;648(1):105-112.
56. Baryshnikova OK, Williams TC, Sykes BD. Internal pH indicators for biomolecular NMR. *J Biomol NMR*. 2008;41(1):5-7.
57. Orgovan G, Noszal B. Electrodeless, accurate pH determination in highly basic media using a new set of H-1 NMR pH indicators. *J Pharm Biomed*. 2011;54(5):958-964.
58. Shchepin RV, Barskiy DA, Coffey AM, et al. (15)N Hyperpolarization of imidazole-(15)N2 for magnetic resonance pH sensing via SABRE-SHEATH. *ACS Sens*. 2016;1(6):640-644.
59. Xiao C, Hao F, Qin X, Wang Y, Tang H. An optimized buffer system for NMR-based urinary metabonomics with effective pH control, chemical shift consistency and dilution minimization. *Analyst*. 2009;134(5):916-925.
60. Chacko VP, Weiss RG. Intracellular pH determination by 13C-NMR spectroscopy. *Am J Physiol*. 1993;264(3 Pt 1):C755-C760.
61. Gillies RJ, Liu Z, Bhujwalla Z. P-31-Mrs measurements of extracellular Ph of tumors using 3-aminopropylphosphonate. *Am J Physiol*. 1994;267(1):C195-C203.
62. Cox N, Kuemmerle R, Millard P, et al. Integrated pH measurement during reaction monitoring with dual reception H-1-P-31 NMR spectroscopy. *Anal Chem*. 2019;91(6):3959-3963.
63. Li M, Meng F, Tsutsumi Y, et al. Understanding molecular interactions in rafoxanide-povidone amorphous solid dispersions from ultrafast magic angle spinning NMR. *Mol Pharm*. 2020;17(6):2196-2207.
64. Lu XY, Skomski D, Thompson KC, McNevin MJ, Xu W, Su Y. Three-dimensional NMR spectroscopy of fluorinated pharmaceutical solids under ultrafast magic angle spinning. *Anal Chem*. 2019;91(9):6217-6224.
65. Lu X, Tsutsumi Y, Huang C, et al. Molecular packing of pharmaceuticals analyzed with paramagnetic relaxation enhancement and ultrafast magic angle pinning NMR. *Phys Chem Chem Phys*. 2020;22:13160-13170.
66. Hirsh DA, Wijesekara AV, Carnahan SL, et al. Rapid characterization of formulated pharmaceuticals using fast MAS H-1 solid-state NMR spectroscopy. *Mol Pharm*. 2019;16(7):3121-3132.
67. Zhang RC, Mroue KH, Ramamoorthy A. Proton-based ultrafast magic angle spinning solid-state NMR spectroscopy. *Accounts Chem Res*. 2017;50(4):1105-1113.
68. Nishiyama Y. Fast magic-angle sample spinning solid-state NMR at 60-100kHz for natural abundance samples. *Solid State Nucl Magn Reson*. 2016;78:24-36.